Short Communication

A first approach on the assessment of the creep behavior of MoTaNbV$_x$Ti high entropy alloys by indentation testing

A. E. Karantzalis[1] · D. Sioulas[1] · A. Poulia[1] · C. Mathiou[1] · E. Georgatis[1]

Received: 19 February 2020 / Accepted: 15 April 2020 / Published online: 23 April 2020

Abstract
MoTaNbV$_x$Ti refractory high entropy alloys were tested with dynamic indentation technique in order to assess their creep behavior. The loading rate was kept constant and three indentation depths were applied. It was found that, by increasing the indentation depth and the V content of the alloys, the stress exponent was reduced. This reduction was associated with the maximum applied stress at the peak load before the holding period and the increase of lattice distortion parameter with increasing the V content.

Keywords Refractory high entropy alloys · Dynamic indentation · Creep assessment · Stress exponent

1 Introduction

During the last decades, high entropy alloys (HEAs) were introduced as a new class of metallic materials with a great potential for various industrial and structural applications. HEAs were developed upon the basis of combining multiple metallic elements (at least five) at almost similar compositional contribution (equi-atomic or near equi-atomic element participation), so that simple solid solution microstructures could be obtained. This approach was adopted based on the novel concept of high entropic content [1].

This new alloy designing direction, far beyond the conventional metallurgy frame, led to the development of new systems with exceptional properties and opened new horizons in the field of metallic systems. Ever since their appearance, various systems of both 3d transition metal and refractory metal HEAs were developed and assessed as far as various physical, chemical and mechanical properties are concerned [1].

Among the mechanical properties, creep resistance is considered to be of the most crucial one for various industrial applications for both conventional and advanced alloys. Under this frame, the creep behavior assessment of HEAs could not be excluded.

Creep behavior assessment was, for many decades, based on careful designing and performing experimental testing, based on typical tensile testing apparatus, providing significant information of vital importance for the material performance, especially at extreme servicing conditions. Nevertheless, the use of dynamic indentation techniques in the assessment of creep response, along with other mechanical properties was eventually and successfully introduced.

Among the advantages of the indentation techniques, the simplicity of the testing procedure, the simplicity of the size and geometry of the required samples and the overall short duration of the experiments, should be addressed. The complexity of the stress fields being developed on the material during indentation, however, led to the requirement/demand of careful and precise evaluation of the involved testing parameters both at experimental and theoretical level [2, 3].

The first systematic presentation of the creep behavior of various materials assessed by indentation techniques was introduced by Li et al. [4]. In the beginning of their

✉ A. E. Karantzalis, akarantz@uoi.gr | [1]Department of Materials Science and Engineering, University of Ioannina, 45110 Ioannina, Greece.

SN Applied Sciences (2020) 2:950 | https://doi.org/10.1007/s42452-020-2761-9

approach, these researchers defined two distinctive areas underneath the indenter: an area of hydrostatic pressure, where no plasticity can happen, followed by an elastic—plastic area where plastic deformation can be expressed and as such creep phenomena can be accumulated.

Li et al. [4] proposed several creep mechanisms: (a) dislocation glide due to high stresses being developed within the elasto-plastic region, prevailing especially at low temperatures, (b) power law dislocation climb—glide mixed mode at more elevated temperatures governed mainly by the higher temperatures, (c) power law breakdown of dislocation climb to a mixed climb—glide mode if, apart from the higher temperatures, high stresses are also present and (d) diffusion creep where the differences in the stress fields between the hydrostatic zone and the elastic–plastic zone, establish chemical potential gradients that lead to atomic diffusion and material flaw from the hydrostatic region underneath the indenter towards the elastic–plastic area close to the sample surface. This statement stands for volume diffusion in the case of single crystal material since, in the case of polycrystalline samples, material flow is accommodated by grain boundary diffusion induced sliding. What is quite remarkable in the approach of Li et al. [4] is the fact that only the last mechanism seems to be dependent on the externally applied load. It is, however, important to notice that in this work, the effect of the pre-creep stage by means of loading rate was not examined.

As Li et al. [4] and other workers ever after showed, grain size, applied load/indentation depth, loading rates and creep holding time are the most crucial parameters that affect the creep response of a material. These parameters were, in a way, formulated for the creep response assessment, in factors such as the Indentation Size Effect (ISE) and the Loading Rate Sensitivity (LRS) and used in various different cases as in the works of Zhang et al. [5], Ding et al. [6], Lin et al. [7], Choi et al. [2] and Ma et al. [8, 9].

As far as the indentation creep assessment of HEAs is concerned, significant amount of research work has been conducted. Interestingly, most of these efforts are mainly focused on FCC structure based HEAs. It was generally observed that the creep behavior of this class of materials, at the holding stage, was very sensitive on the loading rate, the applied force, the depth of penetration and the testing environment temperature. All these factors seem to affect multiple transitions between various mechanisms of material flaw such as dislocation glide, dislocation climb, self-diffusion and it is the domination of one of these factors and/or their combination that determines the overall creep response [5, 9–12]. Although considerable research effort has been focused on the indentation creep behavior of FCC based HEAs, almost negligible work has been conducted on BCC systems. Indicatively, Ma et al. [9] examined the creep behavior of high entropy alloys films of both FCC and BCC structures. They showed that there is a remarkable difference in the creep behavior between the FCC HEA (CoCrFeNiCu) and the BCC alloy ($CoCrFeNiCuAl_{0.25}$). They related these differences by means of edge and screw dislocation different mobility for the BCC system and the required for dislocation nucleation activation volume differences between the two crystal structures.

The present effort is—at the best of the authors' knowledge—the first attempt to evaluate of creep response of Refractory High Entropy Alloys (RHEAs) of the $MoTaNbV_xTi$ system, through the use of indentation techniques. The selected system is the first of a wide project of the authors' research work on the indentation creep behavior of refractory high entropy alloys based on the major MoTaNb core. Systems such as MoTaNbVW, MoTaNbZrTi, MoTaNbHfZrTi are currently being tested.

2 Experimental procedure

2.1 Materials and methods

Vacuum Arc Melting (VAM) was used as the production technique of the $MoTaNbV_xTi$ (x = 0.25, 0.50. 0.75 at.%) refractory high entropy alloys. The melting furnace was equipped with a Ti-getter, while high-purity argon atmosphere was also ensured. A Scanning Electron Microscope (JEOL 6510 LV) equipped with backscattered electron (BSE) and energy dispersive spectroscopy (EDS, x-Act Oxford Instruments) detectors was used for the microstructural investigation of the produced systems, while an X-ray diffractometer (Bruker, D8 Advance) with Cu K_α radiation, ranging from $2\theta = 10°–120°$ and a scanning rate of 0.01°/s tested the alloys' crystal structure.

Dynamic indentation tests were performed using a Shimadzu DUH-211S nano-indenter with a standard Berkovich diamond tip at room temperature. Initial machine calibration was conducted on a fused silica standard to ensure the validity of the testing data. In order to remove the thermal effect, thermal drift was maintained at 0.05 nm s^{-1} during each test. The load holding time was settled as 10 s, to determine whether a creep behavior occurred. Three indentation depth limits for each indent, (deep at 2000 nm, medium at 1000 nm and shallow at 500 nm) were selected, while the strain rate was kept constant at 0.05 s^{-1}. Average values and standard deviation were calculated based on at least 10 trials for each specimen.

2.2 Calculations

For the necessary calculations to be conducted, the approach of Zhang et al. [5] was adopted, with certain modifications been performed when requested.

For a typical nanoindentation test using a Berkovitch indenter, the strain rate and hardness as a function of the indentation depth, are given by the following equations:

$$\dot{\varepsilon} = \frac{1}{h}\frac{dh}{dt} = \frac{\dot{h}}{h} \tag{1}$$

$$\text{and} \quad H = \frac{P}{24,5h^2} \tag{2}$$

where $\dot{\varepsilon}$ is the strain rate, h the indentation depth as a function of time, H is the hardness and P the applied load as the function of time.

During the holding time, the indentation displacement due to creep can be easily approached by adopting the Wang et al. [12] proposed protocol, slightly modified where necessary, and a fitting curve as follows can be obtained:

$$\Delta h(t) = h(t) - h_0 = at^p + kt \tag{3}$$

where h(t) is the indentation depth as a function of the holding time, h is the indentation depth at the onset of the holding time, t is the holding duration, a, p and k are the fitting parameters.

Additionally, as Li et al. [4] and Yu et al. [13] proposed, the indentation creep obeys an empirical power law of the form:

$$\dot{\varepsilon} = \mathrm{A}\sigma^n exp\left(-\frac{Q}{RT}\right) \tag{4}$$

where A is a constant, n is the creep stress exponent, σ the applied stress, Q the activation energy.

The last simple equation useful for the overall approach proposed by Zhang et al. [5], is:

$$\sigma = cH \tag{5}$$

where c is a parameter related to the tested material. By combining Eqs. (1) and (4), it is obtained that:

$$\frac{1}{h}\frac{dt}{dh} = A\sigma^n \exp\left(-\frac{Q}{RT}\right) \tag{6}$$

The introduction of Eq. (5) in Eq. (6) gives:

$$\frac{1}{h}\frac{dh}{dt} = Ac^n H^n \exp\left(-\frac{Q}{RT}\right) \tag{7}$$

Furthermore, by introducing Eq. (2) in Eq. (7), it is obtained

$$\begin{aligned} &\frac{1}{h}\frac{dh}{dt} = Ac^n\left(\frac{P}{24,5h^2}\right)^n \exp\left(-\frac{Q}{RT}\right) \Rightarrow \\ &\frac{1}{h}\frac{dh}{dt} = A\left(\frac{c}{24,5}\right)^n \left(\frac{P}{h^2}\right)^n \exp\left(-\frac{Q}{RT}\right) \end{aligned} \tag{8}$$

where A and c are constants and as such they let us simply define $A\left(\frac{c}{24,5}\right)^n = B$.

Similarly, since the tests were conducted at ambient temperature, then $\exp\left(-\frac{Q}{RT}\right)$ is also constant and let us define $exp\left(-\frac{Q}{RT}\right) = D$. Equation (8) then becomes:

$$\frac{1}{h}\frac{dh}{dt} = B\left(\frac{P}{24,5h^2}\right)^n \mathrm{D} \tag{9}$$

By applying logarithm at both sides of the equation, it is obtained that:

$$ln\left(\frac{1}{h}\frac{dh}{dt}\right) = lnB + nln\left(\frac{P}{h^2}\right) + lnD \tag{10}$$

where lnB and lnD are also constant and as such it can be assumed that lnB + lnD = E and Eq. (10) becomes:

$$ln\left(\frac{1}{h}\frac{dh}{dt}\right) = E + nln\left(\frac{P}{h^2}\right) \tag{11}$$

A plot of $ln\left(\frac{1}{h}\frac{dh}{dt}\right)$ and $ln\left(\frac{P}{h^2}\right)$ is a line with slope equal to the stress exponent n.

In this way the stress exponent n can be calculated. The values of the parameters h, dh/dt can be refined by the outcome of the fitting curve of Eq. (3). The other mechanical properties also calculated in the present work, such as hardness and modulus of elasticity, were calculated by the adopting the approach of Oliver and Pharr [14].

3 Results and analysis

Figure 1 presents the SEM images of the different alloy microstructures along with their XRD analysis. It can be observed that, in all cases, the alloys show a significant degree of segregation and consist practically of two phases: a major primary white phase of a dendritic morphology and an inter-dendritic dark phase. EDS analysis on selective areas of the different systems (Table 1), clearly shows that the white phase is rich in Mo, Ta, Nb and V whereas the dark phase is consisted of mainly Ti. The XRD analysis (Fig. 1 and Table 1) seems to confirm the EDS analysis results, depicting phases of BCC and HCP crystal structure. Table 1 also includes information of one of the most important parameters of HEAs, that of lattice distortion **δ**. In HEAs, the multi-nature of the participating elements leads to the formation of a heavily distorted lattice of high restored elastic energies. This severe lattice distortion is considered to be an intensive strengthening factor

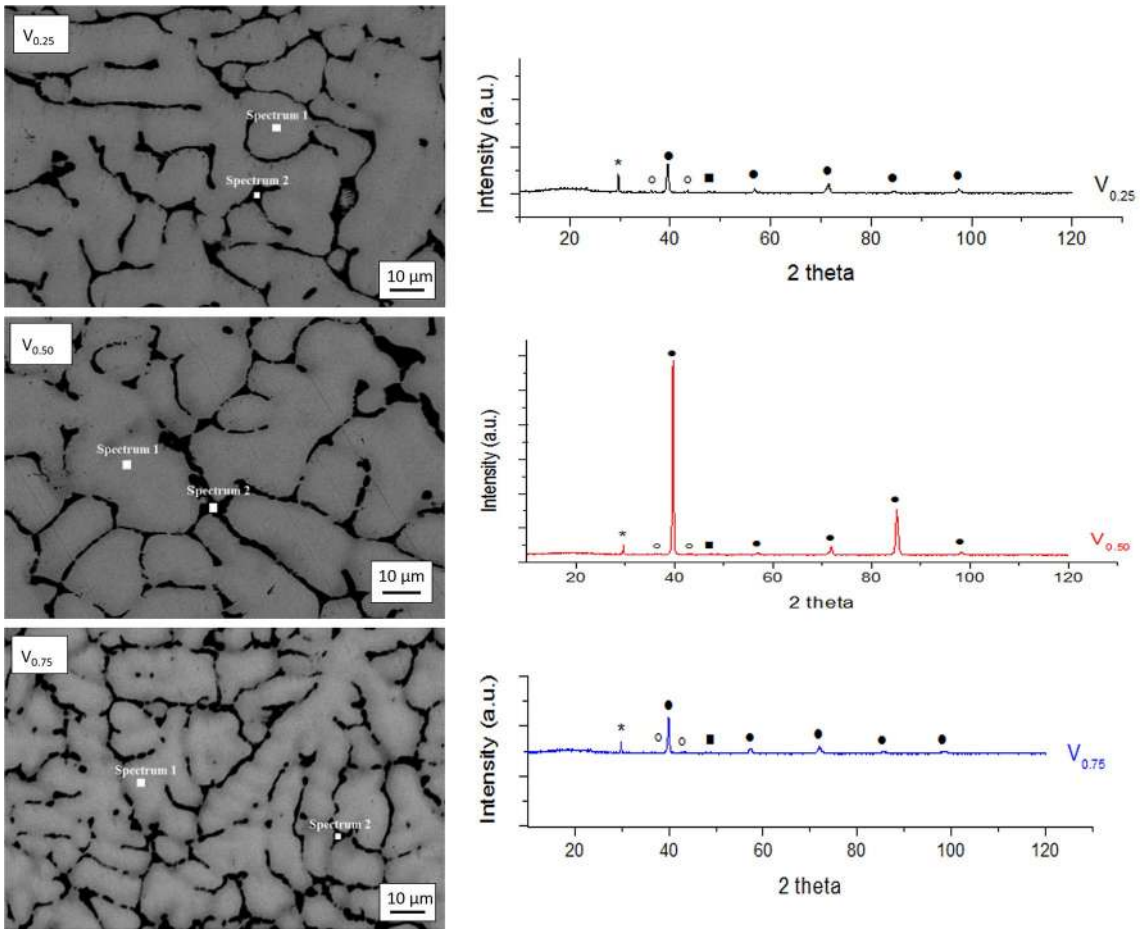

Fig. 1 SEM images of the different alloys produced. Two phases are observed: a primary dendritic white phase and an inter-dendritic dark phase. XRD analysis shows that the primary phase is a BCC solid solution and the dark phase a HCP Laves phase (asterisk Ti oxides, circle hexagonal C14 Laves, filled square cubic C15 Laves, filled cube cubic Im3m)

for HEAs [1]. Therefore, high values of lattice distortion in HEAs, will lead to elevated mechanical properties and reduced ductility, yet, the effect of this severe lattice distortion has not been exploited as far as the creep behavior of HEAs, especially of BCC structure. It can be observed that, from the data of Table 1, as the V content increases, the lattice distortion **δ** also increases for both the primary and the inter-dendritic phases. This observation implies that the complexity of the lattice is increased and so are the obstacles on the successful dislocation movement.

Table 1 also provides information on the fundamental mechanical properties such as Modulus of Elasticity (E) and Hardness (H) assessed by the nano-indentation testing according to the standard Oliver–Pharr approach [14]. It can be observed that that for all the different alloy compositions, the hardness is reduced as the indentation depth increases. This observation is in agreement with other research efforts [11, 15]. As Milmann et al. [15] proposed and Jiao et al. [11] also adopted, this behavior is associated with the fact that at shallow indentation depths, the dislocation density with the elastic–plastic zone underneath the indentation surface is significantly high leading to hardening effect and thus to a higher hardness values. Data of Table 1 also depicts a slight reduction in the modulus of elasticity with increasing the indentation depth. Similar behavior was also reported by Xiao et al. [16] and Jiao et al. [11] and was attributed to dislocation pile up which results in small differences in contact stiffness. It has to be mentioned, however, that Jiao et al. [11] and Xiao et al. [16] in their works refer to small reductions in the modulus of elasticity, whereas in the present case these reductions are more significant. This is due to the fact that E, in the present effort, was calculated after the completion of the creep—holding time stage which depicts that the pile up effect mentioned previously has been developed in a much greater extent.

Figure 2a–c shows the load–displacement curves of the of the white (primary) phases for the different indentation depths and the different V content alloys and Fig. 2d presents the same curves of the dark phase for the 500 nm

Table 1 Chemical composition (at.%) of the refractory alloys produced and calculated values of the lattice distortion, hardness, modulus, stress at the onset of creep stage and stress exponent n

V content (at. %)		Element at.%		Lattice distortion δ	Displacement depth (nm)	Hardness (GPa)	Modulus (GPa)	Stress (maximum load, MPa)	Stress exponent, n
0.25 V	White phase (primary) Sp1	Mo	26.07	2.96	500	9.0 ± 1	200 ± 5	7396.6595	45.00
		Ta	26.06						
		Nb	24.29		1000	7.6 ± 0.6	173 ± 4	5744.8758	44.57
		V	5.18						
		Ti	18.47		2000	7.0 ± 0.2	155 ± 2	5546.8239	40.20
	Dark phase (inter-dendritic) Sp2	Mo	2.63	1.21	500	11.0 ± 2.0	210 ± 4	7751.3112	38.00
		Ta	4.39						
		Nb	7.51						
		V	0.00						
		Ti	85.46						
0.50 V	White phase (primary) Sp1	Mo	27.23	3.19	500	10.0 ± 2.0	215 ± 9	7724.2312	42.00
		Ta	25.68						
		Nb	22.53						
		V	9.50		1000	8.0 ± 1.3	161 ± 4	5943.7186	36.81
		Ti	15.05		2000	7.0 ± 0.3	146 ± 2	5447.9069	27.80
	Dark phase (inter-dendritic) Sp2	Mo	3.40	2.46	500	10.0 ± 2.0	207 ± 3	8104.4905	44.00
		Ta	3.97						
		Nb	7.29						
		V	5.79						
		Ti	79.56						
0.75 V	White phase (primary) Sp1	Mo	24.49	3.51	500	10.0 ± 2.0	195 ± 7	7703.0088	38.00
		Ta	24.06						
		Nb	21.48		1000	7.8 ± 0.4	158 ± 5	6386.5486	36.81
		V	14.88						
		Ti	15.09		2000	7.1 ± 0.2	155 ± 3	5575.2610	30.70
	Dark phase (inter-dendritic) Sp2	Mo	1.69	2.57	500	10. ± 1.0	192 ± 7	7872.9271	36.00
		Ta	3.29						
		Nb	5.38						
		V	7.09						
		Ti	82.55						

indentation depth examined in the present effort. It has to be noticed at this point, that the other indentation depths (1000 and 2000 nm respectively) were not possible to be assessed due to the restricted extent of the inter-dendritic area, inhibiting in this case the focusing of the indentation procedure strictly within them.

Prior to evaluate the actual creep behavior of the various systems during the holding stage, it is very important to examine the pre-holding stage, i.e. the loading stage before the actual creep. This stage is considered to be of high importance and the material response during this step will affect dramatically the next step of creep response [5–10]. Close examination of the loading stage in Fig. 2a–c shows that in all systems and for all the different indentation depths, no significant traces of pop-in events are evident. Pop-in events are practically expressed in the form of incremental displacements upon loading forming the so-called serration morphology. The presence of these serrations are considered to be a strong evidence that creep phenomena are taking place during the loading stage providing a considerable amount of related deformation and, even more importantly, they drain out the creep deformation potential of the material during the actual creep stage, i.e. the holding stage. The most important factor influencing the formation of serrations is the strain rate. Various research efforts have shown that high strain rates during loading stage result in absence of serrations i.e. lack of creep deformation during loading [5–11]. On the contrary, low strain rates usually lead to serration formation and creep deformation [5–11]. The reason for this behavior is that at high strain rates the dislocation generation is also high, yet the applied stress is not adequate enough to activate a slip plane in order for a dislocation to move. Multiple slip planes have to be activated for dislocation movement to commence. However, the high strain rate does not provide adequate time for this activation. In simple words at high strain rates, dislocations can multiply but not move. In this case the loading stage curve appears quite smooth [5]. Furthermore, when no creep deformation is observed in the loading stage, the system will express its creep potential during the holding stage. In the present effort since no serrations are observed, it was expected that the overall creep deformation would take place during the holding period.

The second important observation from the curves of Fig. 2a–c, is the lack of pop-out events, i.e. no serrations or sudden displacement changes during the un-loading stage. Pop-out events are associated with deformation phenomena caused by phase transformations [2–7]. Therefore, since the un-loading stage, in the present effort, is characterized by significant smoothness, it can be postulated that the deformation phenomena developed during the overall testing procedure are governed by dislocation movement issues. Similar conclusions have also been drawn in other research efforts [5].

Figure 3 shows the time–displacement behavior of the primary white phase for the different V compositions and the different indentation depths. Close examination of these curves, reveals the following interesting points:

(a) Irrespectively of the systems, as the preset indentation depth increases, the creep displacement increases.
(b) The creep rate seems to be high in the beginning of the holding (creep) stage and gradually decreases towards the completion of the holding stage. Additionally, it is also evident that the rate of the creep displacement at the end of the holding time increases as the penetration depth increases.
(c) At low penetration depths (500 and 1000 nm), the V content does not seem to have a profound effect on the overall creep displacement and the observed creep displacement rates.

These observations provide useful information for the effort to explain the possible creep mechanisms. In order, however, to postulate these mechanisms, the results presented in Fig. 4 are very important. Figure 4 presents a typical indentation displacement (Δh) vs time (t) curve for the holding stage (creep stage) along with the typical correlation parameters. These correlation parameters were received applying a power law fitting. This observation is very important. It has been proposed by many researchers that a power law fitting of the creep displacement as a function of the holding time, suggests a dislocation driven creep deformation and more specifically that of a dislocation glide mode [2, 5, 9, 11, 12, 17]. Despite of the fact that Li et al. [4] in their early work pointed out that a power law creep behavior is mainly associated with dislocation climb and/or dislocation climb-glide mixed mode at intermediate to high temperatures, in their concluding remarks they do admit that at low temperatures dislocation glide induced plasticity must be the predominant mechanism due to the high stresses being developed within the elastic- plastic zone. As such, in the present effort, since a power law of extremely good fitting was observed, dislocation glide is considered as the main creep deformation mechanism. Additionally, all tests were performed within the interior of primary (dendritic) grains or inter-dendritic areas, far away from the interfacial regions in each case. This testing approach, implies that deformation mechanisms related to grain boundaries must be neglected and the overall analysis should be treated as single crystal creep behavior.

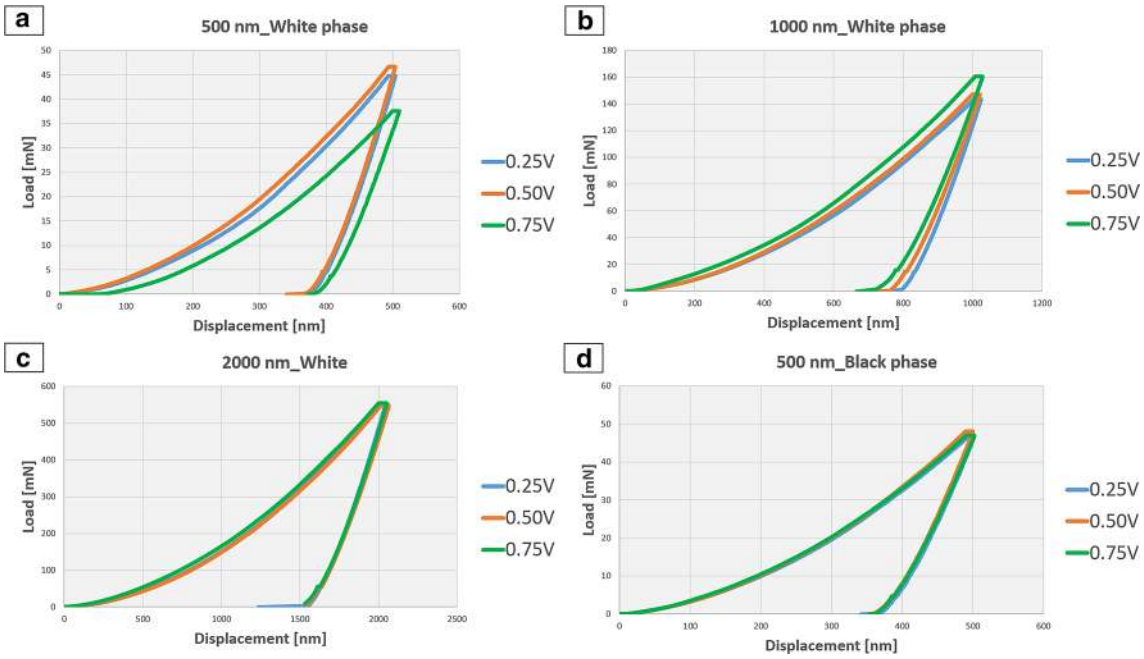

Fig. 2 **a–c** Loading–unloading curves of the white (primary) phases for the different indentation depths and the different V content alloys; **d** loading–unloading curve for 500 nm indentation depth of the dark inter-dendritic phase for the different alloys

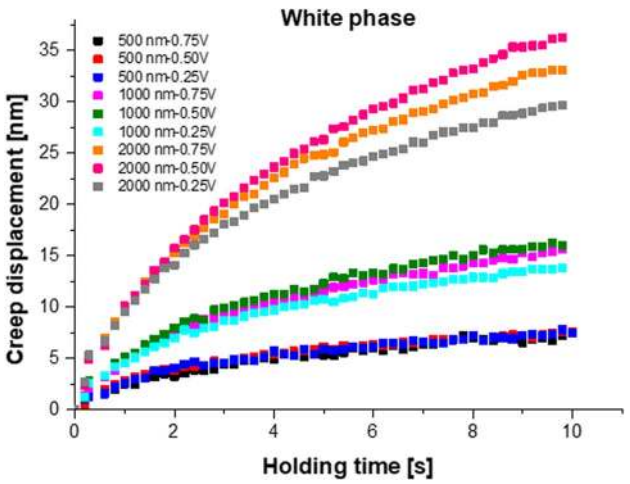

Fig. 3 The indentation displacement as a function of time during the holding (creep) stage of the indentation tests for the white phase at different depths (loads) for all the tested alloys

To obtain an even better and in depth assessment of the creep behavior, the calculation of the stress exponent **n** is required. An example of the **n** exponent calculation, is presented Fig. 5, which shows a typical ln [(1/h)(dh/dt)] versus ln (P/h^2) plot, the slope of which provides the stress exponent **n**. It has been mentioned, in the introduction section, that the exponent **n** has been approached in many different ways and was related to various crucial both testing (loading/strain rate, indentation depth) and material (grain size, nanocrystallinity, amorphicity) parameters, leading in some extent to certain confusion. In the present effort, since a constant loading rate was adopted in all cases and since a single crystal approach was insured, exponent **n** expresses the level of creep strain rates being developed at a given stress, as Ma et al. [9] proposed. Ma et al. [9], Lin et al. [7], Zhang et al. [5] and Zhao et al. [17] treated the exponent **n** as the reverse of the strain rate sensitivity factor m, i.e., n = 1/m. This practically implies that the higher the exponent **n** the less the strain rate sensitivity. It was shown previously, based on curves of Fig. 3**,** that especially in the case of 1000 and 2000 nm of indentation depth, the rate of deformation is very high in the beginning of the loading stage and is gradually reduced towards the end of the holding time. It is also evident that the rate of the creep displacement in the case of 2000 nm at the end of the holding time is higher than in the case of the 1000 nm and 500 nm respectively. This practically implies that the strain rate sensitivity is increased as the loading depth increases. This tendency is mirrored by the obtained values of exponent **n**, as presented in Table 1. In all cases of the different alloy systems the **n** exponent decreases as the indentation depth increases. This observation is quite interesting, as in the most cases of FCC HEAs, the exponent **n** increases with indentation depth and as such the strain sensitivity is reduced [5, 9–11]. Ma et al. [9] reported in their work that the BCC high entropy alloy deposits showed a limited variation in the exponent factor with indentation depth, whereas for the FCC deposits

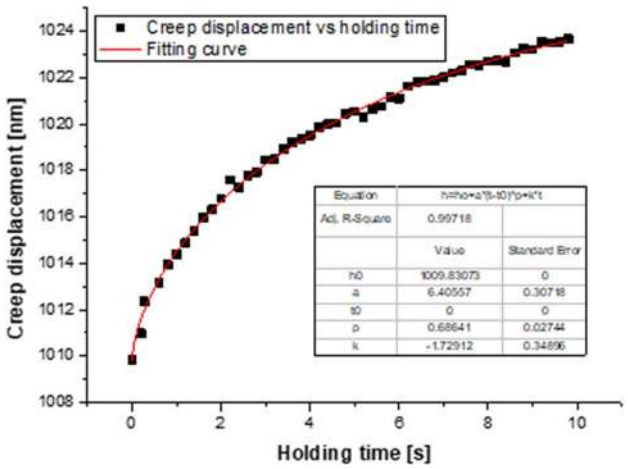

Fig. 4 Typical displacement—time curve showing the power law fitting parameters

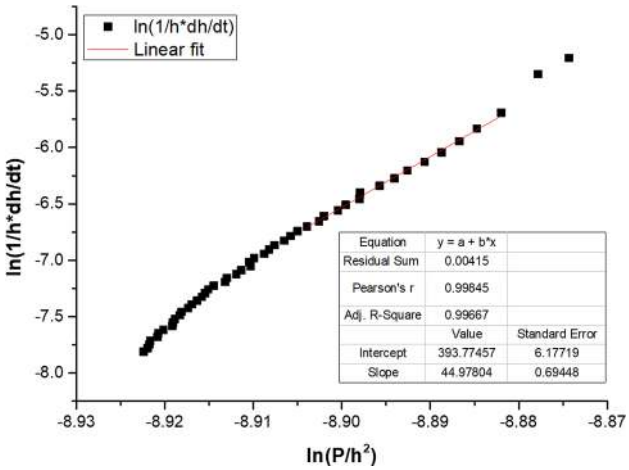

Fig. 5 Typical ln [(1/h)(dh/dt)] versus ln (P/h^2) plot, the slope of which provides the stress exponent n

a significant increase of **n** with depth was observed. It is thus, expected that the BCC HEAs examined in the present effort does not follow the trend that FCC systems show. The important difference with the work of Ma et al. [9] and other works dealing with FCC alloy thin films [8, 9] is the grain size of the tested material. Ma et al. [9] dealt, even in the case of BCC systems, with nano-crystalline deposits and as such the grain size plays an important role on the overall deformation process.

A logic explanation for this different behavior, can arise by the data of Table 1. It can be seen that in all cases the deeper the indentation depth the lower the applied stress (in the form of hardness value) at the peak load at the onset of the holding stage. This practically implies that the dislocation movement potential is reduced as the applied stress causing their motion is reduced. In other words, at higher indentation depths were the applied stresses are lower, the dislocation movement is more sensitive (lower **n**) to any potential stress alteration that could enhance their mobility. Interestingly, Li et al. [4] provided another aspect of the creep behavior at low indentation depths. They observed that in Al at shallow depths of indentation, a diffusion based mechanism can also be activated leading to material flow and thus high creep deformation. This observation by itself cannot stand for the present case, however, Kang et al. [10] observed that during dislocation glide within the distorted lattice of the CoCrFeMnNi alloy they examined, extensive diffusion of atoms was taking place from the bulk of the lattice to the area below the dislocation line, in an effort of the lattice to be relieved. Noteworthy, though, that their experiments were conducted at intermediate temperatures. The outcome of these two works is that diffusion based creep at low indentation depths where the atomic movement paths are short, is possible especially if the strong "need" of the distorted lattice to be relieved is taken into consideration. The authors do admit, however, that the last point is mostly a speculation and further experimentation is required to clarify this issue. It has to be mentioned, at this point, that the literature in many cases [5–12] shows an increase of the stress exponent with the indentation depth which seems to contradict the present findings. However, most of these efforts have been conducted in FCC systems either of plain metallic elements, or common FCC alloys or even HEAs, where the dislocation movement can show different behavior in comparison with BCC systems. Additionally, in most of these efforts there is no thorough examination of the loading stage and the plasticity response of the material during this stage.

A closer examination of the data in Table 1, reveals another interesting point; the reduction of exponent **n** becomes more profound in the case of the 0.50 and 0.75% V alloys. By comparing the stress values at the maximum load for the different V contents, it can be seen that for a given depth of penetration, the stress levels do not differ significantly, yet the **n** exponent changes especially in the case of 1000 and 2000 nm depth. It is thus believed that, apart from the stress reduction mentioned previously, other phenomena must account for this significant reduction. Since the stresses are more or less the same, the authors believe that exponent **n** acquires a new meaning and content and is related to the obstacles preventing the dislocation movement. As Table 1 shows, lattice distortion **δ** must play a crucial role towards this direction. Li et al. [4] early postulated that in dislocation glide induced deformation, the dislocations that move in a single crystal meet various obstacles (solute atoms or precipitates) that they have to cut-off or

bypass. The more the obstacles, the more restricted their motion and the less the creep deformation. In HEAs, lattice distortion **δ** is an indirect measure of the complexity of the lattice and the extent of the obstacles inhibiting the dislocation movement. Therefore, the higher the **δ** parameter the more restricted the dislocation mobility, the more reduced the creep rate, the more reduced the **n** exponent. At low V content (0.25) hence, lattice distortion is relatively low implying less obstacles for the dislocation movement. As such, even at lower stresses (deeper indentations) dislocations can still move relatively easily. As the V content increases, the effect of the lattice distortion becomes more significant inhibiting more intensively the dislocation movement.

The discussion in the previous paragraphs was referring to the white (primary) phase creep response. As far as the dark (inter-dendritic) phase is concerned, it was not feasible to conduct tests at high indentation depth due to their small size. It can be observed however that, as Table 1 shows, the stress exponent is in general lower than the stress exponents of the white phase, despite the fact that its lattice distortion is significantly lower than those of the white phases. This is due to the fact that the dark phase is a HCP structure, the plasticity potential of which is considerably lower than that of the BCC and the FCC structures. Nevertheless, the authors would like to mention that the exponent **n** of the dark phase is lower than that of the white but not that low as its HCP structure may possibly induce. It is possible that other deformation mechanisms may also contribute such as twinning induced plasticity. Further experimentation is required towards this direction.

4 Conclusions

- $MoTaNbV_xTi$ high entropy alloys were tested as far as their creep response is considered by a dynamic indentation technique
- It was proved that the stress exponent was reduced as the depth of the indentation increased. This reduction was associated with the reduction of the applied stress at the initiation of the creep holding period and the subsequent reduction of the dislocation mobility.
- Lattice distortion increased as the V content increased leading to a reduction of the exponent n. This was attributed to the enhanced obstacles due to the distorted lattice, inhibiting thus further the dislocation mobility.

Compliance with ethical standards

Conflict of interest The author(s) declare that they have no conflict of interest.

References

1. Miracle DB, Senkov ON (2017) A critical review of high entropy alloys and related concepts. Acta Mater 122:448–511. https://doi.org/10.1016/j.actamat.2016.08.081
2. Choi IN, Yoo BG, Kim YJ, Jang JI (2012) Indentation creep revisited. J Mater Res 27:3–11. https://doi.org/10.1557/jmr.2011.213
3. Bull SJ (2005) Nanoindentation of coatings. J Phys D Appl Phys 38:393–413. https://doi.org/10.1088/0022-3727/38/24/R01
4. Li WB, Henshall JL, Hooper RM, Easterling KE (1991) The mechanisms of indentation creep. Acta Metall Mater 39:3099–3110. https://doi.org/10.1016/0956-7151(91)90043-Z
5. Zhang L, Yu PF, Cheng H et al (2016) Nanoindentation creep behavior of an $Al_{0.3}$CoCrFeNi high-entropy alloy. Metall Mater Trans A 47:5871–5875. https://doi.org/10.1007/s11661-016-3469-8
6. Ding ZY, Song YX, Ma Y, Huang XW, Zhang TH (2019) Nanoindentation investigation on the size-dependent creep behavior in a Zr–Cu–Ag–Al bulk metallic glass. Metals 9:613. https://doi.org/10.3390/met9050613
7. Lin PH, Chou HS, Huang JC, Chuang WS, Jang JSC, Nieh TG (2019) Elevated-temperature creep of high entropy alloys via nanoindentation. MRS Bull 44:860–866. https://doi.org/10.1557/mrs.2019.258
8. Ma ZS, Long SG, Zhou YC, Pan Y (2008) Indentation scale dependence of tip-in creep behavior in Ni thin films. Scr Mater 59:195–198. https://doi.org/10.1016/j.scriptamat.2008.03.014
9. Ma Y, Feng YH, Debela TT, Peng GL, Zhang TH (2016) Nanoindentation study on the creep characteristics of high-entropy alloy films: fcc versus bcc structures. Int J Refract Met Hard Mater 54:395–400. https://doi.org/10.1016/j.ijrmhm.2015.08.010
10. Kang YB, Shim SH, Lee KH, Hong SI (2018) Dislocation creep behavior of CoCrFeMnNi high entropy alloy at intermediate temperatures. Mater Res Lett 6:689–695. https://doi.org/10.1080/21663831.2018.1543731
11. Jiao ZM, Chu MY, Yang HJ, Wang ZH, Qiao JW (2015) Nanoindentation characterised plastic deformation of a $Al_{0.5}$CoCrFeNi high entropy alloy. Mater Sci Technol 31:1244–1249. https://doi.org/10.1179/1743284715Y.0000000048
12. Wang Z, Guo S, Wang Q et al (2014) Nanoindentation characterized initial creep behavior of a high-entropy-based alloy CoFeNi. Intermetallics 53:183–186. https://doi.org/10.1016/j.intermet.2014.05.007
13. Yu PF, Feng SD, Xu GS et al (2014) Room-temperature creep resistance of Co-based metallic glasses. Scr Mater 90–91:45–48. https://doi.org/10.1016/j.scriptamat.2014.07.013
14. Oliver WC, Pharr GM (2004) Measurement of hardness and elastic modulus by instrumented indentation: advances in understanding and refinements to methodology. J Mater Res 19:3–20. https://doi.org/10.1557/jmr.2004.19.1.3
15. Milman YV, Golubenko AA, Dub SN (2011) Indentation size effect in nanohardness. Acta Mater 59:7480–7487. https://doi.org/10.1016/j.actamat.2011.08.027
16. Xiao G, Yuan G et al (2014) Strain rate sensitivity of Sn-3.0Ag-0.5Cu solder investigated by nanoindentation. Mater Sci Eng A 613:336–339. https://doi.org/10.1016/j.msea.2014.06.113
17. Zhao J, Wang F, Huang P, Lu TJ, Xu KW (2014) Depth dependent strain rate sensitivity and inverse indentation size effect

of hardness in body-centered cubic nanocrystalline metals. Mater Sci Eng A 615:87–91. https://doi.org/10.1016/j.msea.2014.07.057